MOLECULAR ONCOLOGY 8 (2014) 620–632

available at www.sciencedirect.com

ScienceDirect

www.elsevier.com/locate/molonc

Photoimmunotherapy: Comparative effectiveness of two monoclonal antibodies targeting the epidermal growth factor receptor

Kazuhide Sato[a], *Rira Watanabe*[a], *Hirofumi Hanaoka*[a], *Toshiko Harada*[a], *Takahito Nakajima*[a], *Insook Kim*[b], *Chang H. Paik*[c], *Peter L. Choyke*[a], *Hisataka Kobayashi*[a,*]

[a]*Molecular Imaging Program, Center for Cancer Research, National Cancer Institute, MD 20892, United States*
[b]*Applied/Developmental Research Directorate, Leidos Biomedical Research Inc., Frederick, MD 20892, United States*
[c]*Nuclear Medicine Department, Warren Grant Magnuson Clinical Center, MD 20892, United States*

ARTICLE INFO

Article history:
Received 13 November 2013
Received in revised form
5 December 2013
Accepted 13 January 2014
Available online 22 January 2014

Keywords:
Photoimmunotherapy
Epidermal growth factor receptor
Monoclonal antibody
NIR-fluorescence
Pharmacokinetics

ABSTRACT

Photoimmunotherapy (PIT) is a new cancer treatment that combines the specificity of antibodies for targeting tumors with the toxicity induced by photosensitizers after exposure to near infrared (NIR) light. Herein we compare two commonly available anti-EGFR monoclonal antibodies, cetuximab and panitumumab, for their effectiveness as PIT agents in EGFR positive tumor models. A photosensitizer, IR-700, conjugated to either cetuximab (cet-IR700) or panitumumab (pan-IR700), was evaluated using EGFR-expressing A431 and MDAMB468-luc cells in 2D- and 3D-culture. PIT was conducted with irradiation of NIR light after exposure of the sample or animal to each conjugate. *In vivo* PIT was performed with fractionated exposure of NIR light after injection of each agent into A431 xenografts or a MDAMB468-luc orthotopic tumor bearing model.

Cet-IR700 and pan-IR700 bound with equal affinity to the cells in 2D-culture and penetrated equally into the 3D-spheroid, resulting in identical PIT cytotoxic effects *in vitro*. In contrast, *in vivo* anti-tumor effects of PIT with cet-IR700 were inferior to that of pan-IR700. Assessment of the biodistribution showed lower accumulation into the tumors and more rapid hepatic catabolism of cet-IR700 compared to pan-IR700. Although cet-IR700 and pan-IR700 showed identical *in vitro* characteristics, pan-IR700 showed better therapeutic tumor responses than cet-IR700 in *in vivo* mice models due to the prolonged retention of the conjugate in the circulation, suggesting that retention in the circulation is advantageous for tumor responses to PIT. These results suggest that the choice of monoclonal antibody in photosensitizer conjugates may influence the effectiveness of PIT.

Published by Elsevier B.V. on behalf of Federation of European Biochemical Societies.

Abbreviations: PIT, photoimmunotherapy; EGFR, epidermal growth factor receptor; cet, cetuximab; pan, panitumumab; IR700, IRDye700DX; NIR, near-infrared.

* *Corresponding author*. Molecular Imaging Program, Center for Cancer Research, National Cancer Institute, NIH, Building 10, Room B3B69, MSC1088, Bethesda, MD 20892-1088, USA. Tel.: +1 301 435 4086; fax: +1 301 402 3191.
E-mail address: Kobayash@mail.nih.gov (H. Kobayashi).

1574-7891/$ – see front matter Published by Elsevier B.V. on behalf of Federation of European Biochemical Societies.
http://dx.doi.org/10.1016/j.molonc.2014.01.006

1. Introduction

Epidermal growth factor receptors (EGFR) are commonly expressed on the cell membrane of various cancers and activity of these receptors results in accelerated cell growth and carcinogenesis (Gialeli and Kletsas, 2009; Yamaguchi et al., 2013; Yarden and Pines, 2012). EGFRs are also overexpressed on the cell surface of several cancers including lung, colon, head and neck, and esophageal cancers (Eng, 2010; Markovic and Chung, 2012; Norguet et al., 2012; Stinchcombe and Socinski, 2010; Vecchione et al., 2011); therefore, a variety of targeted molecules have been developed to either block ligand binding, inhibit EGF receptor tyrosine kinases or elicit antibody dependent cellular cytotoxicity (ADCC). Two monoclonal antibodies, cetuximab, a chimeric monoclonal antibody and panitumumab, a total human monoclonal antibody, have been approved by the US FDA and have been widely used for EGFR-expressing cancers (Reichert et al., 2005; Tebbutt et al., 2013; Waldmann, 2003).

Photoimmunotherapy (PIT) is a new cancer treatment based on an antibody-photosensitizer conjugation. PIT conjugates combine the specific antibodies with the toxicity induced by photosensitizers after exposure to near infrared light (Mitsunaga et al., 2012a, 2011). For instance, the photosensitizer, IR700, (a silica based phthalocyanine dye) is conjugated to an antibody and is then activated after cell binding by near infrared (NIR) light at 690 nm. *In vitro* studies have shown PIT to be highly cell-specific, with non-expressing cells immediately adjacent to targeted cells demonstrating no toxic effects. Recent data suggests that once the mAb-IR700 conjugate binds to the target cell and is exposed to NIR light, it can quickly result in rapid and irreversible damage to the cell membrane. Within minutes of exposure to NIR light, the cell membrane ruptures leading to necrotic cell death (Mitsunaga et al., 2012a,b, 2011; Nakajima et al., 2013, 2012; Sano et al., 2013a). While this is a promising treatment, it is still unclear which of the two available anti-EGFR antibodies produces a superior PIT effect.

In this study, we compare the *in vitro* and *in vivo* cell killing efficacy of PIT using either cetuximab-IR700 (cet-IR700) or panitumumab-IR700 (pan-IR700).

2. Material and methods

2.1. Reagents

A water soluble, silicon-phthalocyanine derivative, IRDye700DX NHS ester ($C_{74}H_{96}N_{12}Na_4O_{27}S_6Si_3$, molecular weight of 1954.22) was obtained from LI-COR Bioscience (Lincoln, NE, USA). Cetuximab, a chimeric (mouse/human) mAb directed against EGFR, was purchased from Bristol-Meyers Squibb Co (Princeton, NJ, USA). Panitumumab, a fully humanized IgG_2 mAb directed against EGFR, was purchased from Amgen (Thousand Oaks, CA, USA). All other chemicals were of reagent grade.

2.2. Synthesis of IR700-conjugated cetuximab and panitumumab

Cetuximab or panitumumab (1 mg, 6.8 nmol) was incubated with IR700 NHS ester (66.8 μg, 34.2 nmol, 5 mmol/L in DMSO) in 0.1 mol/L Na_2HPO_4 (pH 8.5) at room temperature for 1 h, as panitumumab was previously described (Mitsunaga et al., 2011). The mixture was purified with a Sephadex G50 column (PD-10; GE Healthcare, Piscataway, NJ, USA). The protein concentration was determined with Coomassie Plus protein assay kit (Thermo Fisher Scientific Inc, Rockford, IL, USA) by measuring the absorption at 595 nm with spectroscopy (8453 Value System; Agilent Technologies, Santa Clara, CA, USA). The concentration of IR700 was measured by absorption at 689 nm with spectroscopy to confirm the number of fluorophore molecules conjugated to each mAb. The synthesis was controlled so that an average of three IR700 molecules were bound to a single antibody. We performed SDS-PAGE as a quality control for each conjugate as previously reported (Sano et al., 2013d). We used diluted cetuximab and panitumumab as non-conjugated controls for SDS-PAGE and the fluorescent bands were measured with a Pearl Imager (LI-COR Biosciences) with a 700 nm fluorescence channel.

2.3. Cell culture

EGFR-expressing A431 cells and MDAMB468-luc cells (stable luciferase-transfected) were used in these experiments (Mitsunaga et al., 2012b, 2011). Cells were grown in RPMI 1640 (Life Technologies, Gaithersburg, MD, USA) supplemented with 10% fetal bovine serum and 1% penicillin/streptomycin (Life Technologies) in tissue culture flasks in a humidified incubator at 37 °C at an atmosphere of 95% air and 5% carbon dioxide.

2.4. Spheroid culture

Spheroids were generated by the hanging drop method (Tung et al., 2011). Five thousand cells were suspended in 50 μL medium and were then dispensed into 96 well plates (3D Biomatrix Inc, Ann Arbor, MI, USA) following manufacture's instructions.

2.5. Fluorescence microscopy

To detect the antigen specific localization of IR700 conjugates, fluorescence microscopy was performed (IX61 or IX81; Olympus America, Melville, NY, USA). Ten thousand cells were seeded on cover-glass-bottomed dishes and incubated for 24 h. Cet-IR700 or pan-IR700 was then added to the culture medium at 10 μg/mL and incubated at 37 °C. The cells were then washed with PBS; Propidium Iodide (PI)(1:2000)(Life Technologies) and Lyso Tracker Red DND-99 (lysotracker, final 75 nM; Life Technologies), were used to detect dead cells, and acidic organelles, respectively (Raben et al., 2009; Smith et al., 2012). PI was added into the media 30 min before PIT. The cells were then exposed to NIR light (2 J/cm^2) and serial images were obtained. The filter was set to detect IR700 fluorescence with a 590–650 nm excitation filter, and a 665–740 nm band pass emission filter.

Immunostaining was performed as previously described (Sato et al., 2011); briefly, the cells were fixed with 3.7% formaldehyde in PBS for 10 min at room temperature followed by permeabilization for 10 min with 0.2% Triton X-100 containing

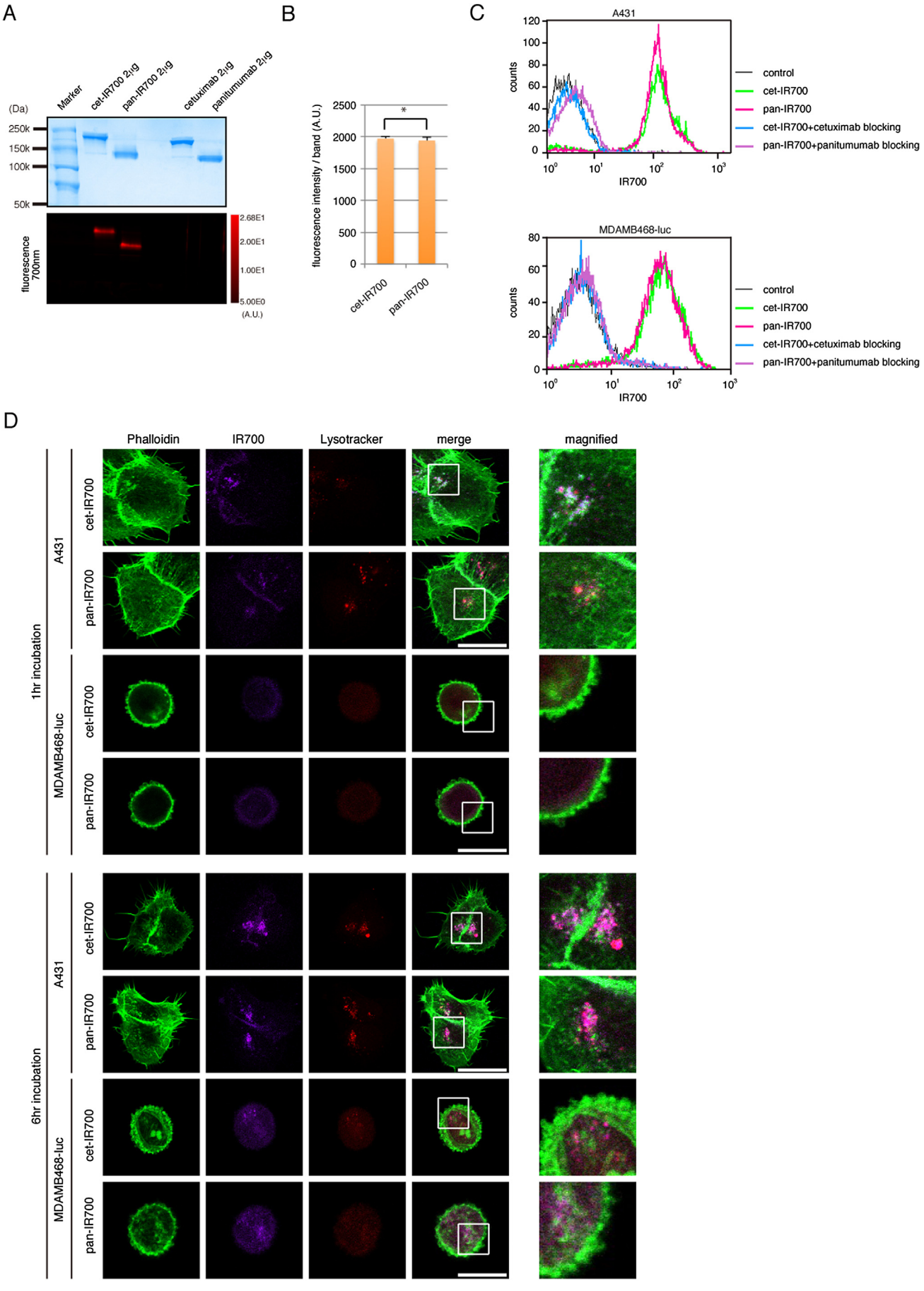
A
Marker
cet-IR700 2μg
pan-IR700 2μg
cetuximab 2μg
panitumumab 2μg
(Da)
250k
150k
100k
50k
fluorescence 700nm
2.68E1
2.00E1
1.00E1
5.00E0
(A.U.)
B
fluorescence intensity / band (A.U.)
2500
2000
1500
1000
500
0
*
cet-IR700
pan-IR700
C
A431
counts
IR700
control
cet-IR700
pan-IR700
cet-IR700+cetuximab blocking
pan-IR700+panitumumab blocking
MDAMB468-luc
D
Phalloidin
IR700
Lysotracker
merge
magnified
1hr incubation
6hr incubation
A431
MDAMB468-luc
cet-IR700
pan-IR700

2 mg/mL BSA. Alexa-fluor488 Phalloidin (Life Technologies) was used to detect actin. The fixed samples were observed with a confocal laser microscope (LSM5 meta, Carl Zeiss, Jena, Germany). Analysis of the images was performed with ImageJ software (http://rsb.info.nih.gov/ij/).

2.6. *Flow cytometry*

Fluorescence from cells after incubation with cet-IR700 or pan-IR700 was measured using a flow cytometer (FACS Calibur, BD BioSciences, San Jose, CA, USA) and CellQuest software (BD BioSciences). A431 and MDAMB468-luc cells (1×10^5) were incubated with each of the conjugates for 1 h at 37 °C. To validate the specific binding of the conjugated antibody, excess antibody (50 μg) was used to block 0.5 μg of dye-antibody conjugates. Furthermore, to elucidate cross reactivity to EGFR, panitumumab-TexRed was used (Nakajima et al., 2013).

2.7. In vitro *photoimmunotherapy*

Two hundred thousand cells were seeded into 12 well plates and incubated for 24 h. Medium was replaced with fresh culture medium containing 10 μg/mL of cet-IR700 or pan-IR700 and incubated for 6 h at 37 °C. After washing with PBS, phenol red-free culture medium was added. Then, cells were irradiated with a red light-emitting diode (LED), which emits light at 670–710 nm wavelength (L690-66-60; Marubeni America Co., Santa Clara, CA, USA), with a power density of 25 mW/cm^2 as measured with an optical power meter (PM 100, Thorlabs, Newton, NJ, USA).

2.8. *Cytotoxicity/phototoxicity assay*

The cytotoxic effects of PIT with cet-IR700 or pan-IR700 were determined by the residual luciferase activity assay and flow cytometric PI staining, which can detect compromised cell membranes. For the luciferase activity assay, 150 μg/mL D-luciferin-containing media (Gold Biotechnology, St Louis, MO, USA) was administered to PBS-washed cells 1 h after PIT, and analyzed on a bioluminescence imaging (BLI) system (Photon Imager; Biospace Lab, Paris, France). For the flow cytometric assay, cells were trypsinized 1 h after treatment and washed with PBS. PI was added in the cell suspension (final 2 μg/mL) and incubated at room temperature for 30 min, followed by flow cytometry.

2.9. *LDH cytotoxicity assay*

The cytotoxic effects of PIT with cet-IR700 or pan-IR700 on A431 spheroids were determined with the Cytotoxicity Detection Kit Plus (Roche Applied Science, Basel, Switzerland), which can detect cell membrane damage. Day7 spheroids, pre-incubated with cet-IR700 or pan-IR700 for 6 h, were washed with PBS, and transferred to 96 well plates (containing PBS), then irradiated with NIR light. 1 h later, the assay was performed. The analysis was done with a VICTOR-X3 plate reader (Perkin Elmer, Woodlands, TX, USA), and calculation of cytotoxicity was made according to manufacturer's instructions. All other procedures were performed following manufacturer's instructions.

2.10. *Animal and tumor models*

All *in vivo* procedures were conducted in compliance with the Guide for the Care and Use of Laboratory Animal Resources (1996), US National Research Council, and approved by the local Animal Care and Use Committee. Six- to eight-week-old female homozygote athymic nude mice were purchased from Charles River (NCI-Frederick). During procedures, mice were anesthetized with isoflurane. Two million A431 cells were injected subcutaneously in the right dorsum of the mice. In order to determine tumor volume, the greatest longitudinal diameter (length) and the greatest transverse diameter (width) were measured with an external caliper. Tumor volumes based on caliper measurements were calculated by the following formula; tumor volume = length × width^2 × 0.5 (Mitsunaga et al., 2011). Tumors reaching approximately 50 mm^3 in volume were selected for the study. Six million MDAMB468-luc cells were implanted into the right mammary fat pads. D-luciferin (15 mg/mL, 200 μL) was injected intraperitoneally into mice 14 days after cell implantation, and analyzed with a Photon Imager for luciferase activity, and then mice were selected for further study based on tumor size and bioluminescence signals.

2.11. In vivo *photoimmunotherapy with cet-IR700 or pan-IR700*

A431 tumor-bearing mice were randomized into 5 groups of at least 10 animals per group for the following treatments: (1) no treatment (control); (2) 100 μg of cet-IR700 i.v. every week, no NIR light exposure (3) 100 μg of pan-IR700 i.v. every week, no NIR light exposure; (4) 100 μg of cet-IR700 i.v. every week, NIR light was administered at 50 J/cm^2 on day 1 after injection and 100 J/cm^2 on day 2 after injection. (5) 100 μg of pan-IR700 i.v. every week, NIR light was administered at 50 J/cm^2 on day 1 after injection and 100 J/cm^2 on day 2 after injection. These therapies were performed every week for up to 2 weeks. Mice were monitored daily, and tumor volumes were measured three times a week until the tumor diameter reached 2 cm, whereupon the mice were euthanized with carbon dioxide. Fluorescence images, as well as white light

Figure 1 – Quality control of cet-IR700 and pan-IR700 synthesis. (A) Validation of cet-IR700 and pan-IR700 by SDS-PAGE (upper: colloidal blue staining, lower: fluorescence). Diluted commercial cetuximab and panitumumab were used as controls. (B) Quantification of fluorescence intensity between cet-IR700 and pan-IR700 (*ns). (C) Specific binding function to EGFR by flow cytometry showing similar binding. (D) A431 and MDAMB468-luc cells were incubated with cet-IR700 or pan-IR700 for indicated times and fixed. Immunostaining was performed with Lyso Tracker (red: lysosome detection) and phalloidin (green: actin detection, especially membrane). Both cet-IR700 and pan-IR700 were internalized into cells in a time dependent manner. Bar = 25 μm.

images, were obtained using a Pearl Imager with a 700 nm fluorescence channel. For analyzing fluorescence intensities, tumors of the same size were compared and regions of interest (ROI) were placed over the entire tumor. Average fluorescence intensity of each ROI was calculated. When comparing fluorescence target-to-background ratio (TBR), ROIs were placed in the adjacent non-tumor region. For the BLI study, mice were randomized into 2 groups of 7 animals per group for the following treatments: (1) 100 μg of cet-IR700 i.v., with NIR light administered at 50 J/cm^2 on day 1 after injection and 100 J/cm^2 on day 2 after injection; (2) 100 μg of pan-IR700 i.v., NIR light was administered at 50 J/cm^2 on day 1 after injection and 100 J/cm^2 on day 2 after injection. NIR light exposure was performed 15 days after cell implantation. Mice images were acquired over time with a fluorescence imager (Pearl Imager) for detecting IR700 fluorescence, and Photon Imager

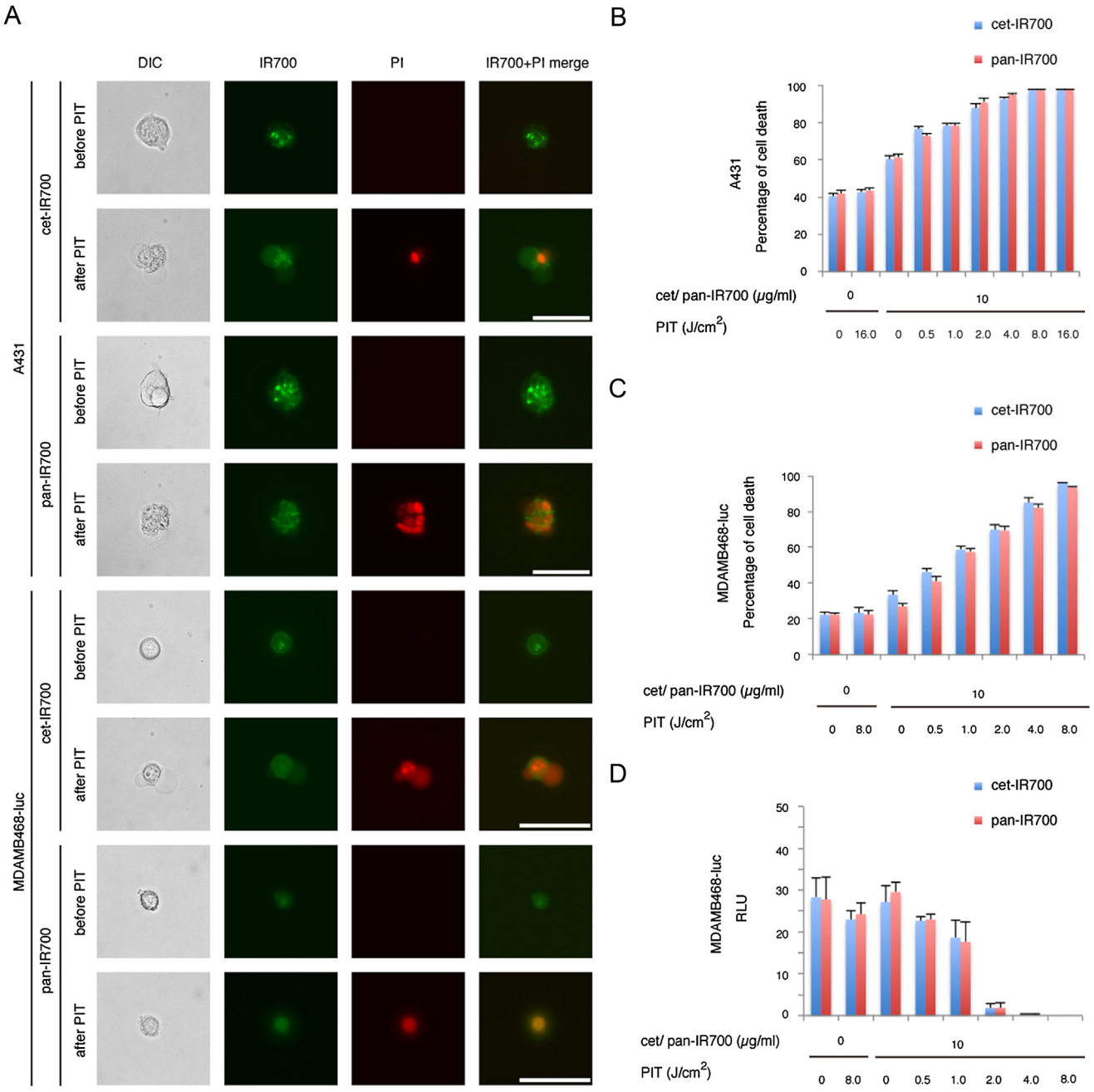

Figure 2 – Microscopy of necrotic cell death and evaluation of cell damage by PIT *in vitro* with cet-IR700 or pan-IR700. (A) A431 and MDAMB468-luc cells were treated with cet-IR700 or pan-IR700 and observed by microscopy (before and after irradiation of NIR light). Necrotic cell death was observed upon excitation with NIR light (After). Bar = 50 μm. PIT-induced cytotoxicity with either cet-IR700 or pan-IR700 in A431 (B) and MDAMB468-luc (C) cells increased in a light dose-dependent manner. There is no significant difference between cet-IR700 and pan-IR700 at any point. (D) Luciferase activity in MDAMB468-luc cells decreased by cet-IR700 or pan-IR700 mediated PIT in a light dose-dependent manner. No significant differences were observed between cet-IR700 and pan-IR700 at any point.

for BLI. For analyzing BLI, ROI of similar size were placed over the entire tumor. When comparing fluorescence TBR, the average fluorescence intensity of each ROI was measured, and ROIs were placed in the adjacent non-tumor region (e.g. a symmetrical region to the left of the tumor). The calculation of TBR has been previously described (Mitsunaga et al., 2011). For measuring the total fluorescence of the tumor region, the ROI of equal size was placed on the tumor and adjacent non-tumor tissue.

2.12. Biodistribution study

A431 tumor bearing mice were divided into two groups ($n = 5$) for biodistribution studies as described previously (Ogawa et al., 2009; Sano et al., 2013b). In brief, ^{125}I-cetuximab and ^{125}I-panitumumab were prepared using the Iodo-Gen procedure and purified with a PD-10 size exclusion column. The specific activities were 410 kBq/μg for cetuximab and 370 kBq/μg for panitumumab. ^{125}I-cetuximab or ^{125}I-panitumumab (37 kBq/5 μg/100 μL in PBS/mouse) was injected via tail vein, and the distribution was determined at 6 h, 1 day, 2 day and 4 day postinjection. Organs were excised, weighed, and the radioactivity counts were measured by a 2480 Automatic Gamma Counter: Wizard^2 (Perkin Elmer), using the injected dose as a standard. The data were shown as the percentage injected dose per gram of tissue (%ID/g).

2.13. Statistical analysis

Data are expressed as means ± s.e.m. from a minimum of four experiments, unless otherwise indicated. Statistical analyses were carried out using a statistics program (GraphPad Prism;

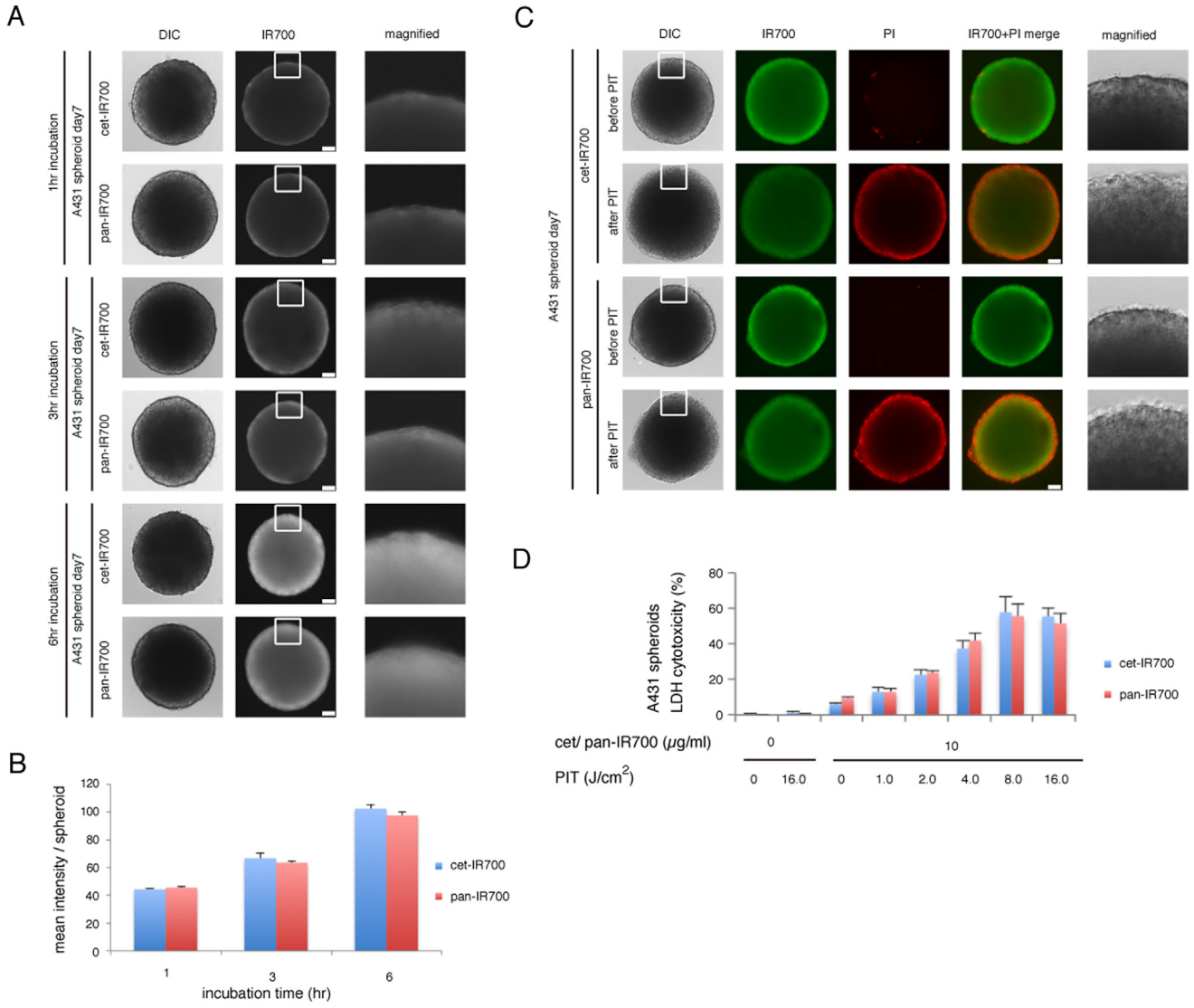

Figure 3 – Permeation of cet-IR700 and pan-IR700 into A431 3D spheroids and the effect on PIT. (A) Permeation of cet-IR700 or pan-IR700 into A431 3D spheroids increased over time. Bar = 100 μm. (B) Quantification of the intensity of IR700 showed no significant difference between cet-IR700 and pan-IR700 ($n = 10$) at any point. (C) A431 3D spheroids were treated with PIT after exposure to either cet-IR700 or pan-IR700 for 6 h and observed by microscopy (before and after irradiation of NIR light). Necrotic cell damage was observed after PIT. Bar = 100 μm. (D) LDH cytotoxicity assay (for the spheroids exposed with cet-IR700 and pan-IR700 for 6 h) showed increasing cell death with increases in light dose. There was no significant difference between cet-IR700 and pan-IR700 in efficacy at any point.

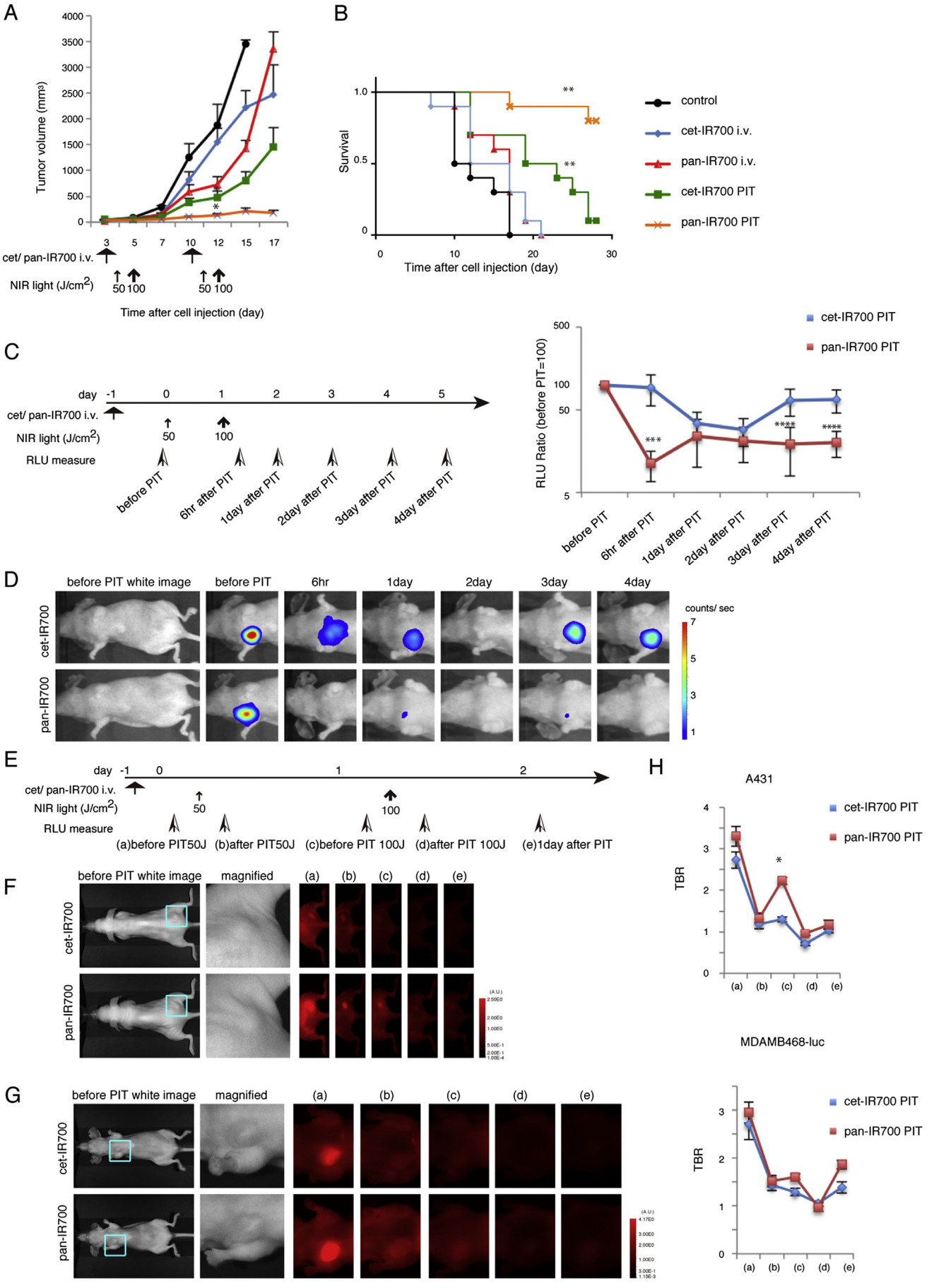
A
Tumor volume (mm³)
cet/ pan-IR700 i.v.
NIR light (J/cm²)
Time after cell injection (day)
B
Survival
Time after cell injection (day)
control
cet-IR700 i.v.
pan-IR700 i.v.
cet-IR700 PIT
pan-IR700 PIT
C
day
cet/ pan-IR700 i.v.
NIR light (J/cm²)
RLU measure
before PIT
6hr after PIT
1day after PIT
2day after PIT
3day after PIT
4day after PIT
RLU Ratio (before PIT=100)
D
before PIT white image
cet-IR700
pan-IR700
counts/ sec
E
(a)before PIT50J
(b)after PIT50J
(c)before PIT 100J
(d)after PIT 100J
(e)1day after PIT
F
magnified
H
A431
MDAMB468-luc
TBR
G

GraphPad Software, La Jolla, CA, USA). For multiple comparisons, a one-way analysis of variance (ANOVA) with post-test (Kruskal–Wallis test with post-test) was used. The cumulative probability of survival was estimated in each group with a Kaplan–Meier survival curve analysis, and the results were compared with the log-rank test and Wilcoxon test. Student's t test was also used to compare the two conjugates; $p < 0.05$ was considered to indicate a statistically significant difference.

3. Results

3.1. In vitro *characterization of cet-IR700 and pan-IR700 conjugates*

To evaluate the properties of cet-IR700 and pan-IR700, SDS-PAGE was performed and read by protein staining and IR700 fluorescence. The bands of IR700-conjugated mAbs were shown at slightly higher molecular weight than non-conjugated controls (diluted mAbs from commercial sources), and fluorescence intensities of both cet-IR700 and pan-IR700 were identical (Figure 1A and B). Next, we examined the fluorescence signals of cet-IR700 and pan-IR700 bound to EGFR-positive cells by FACS. After incubation with either cet-IR700 or pan-IR700, A431 and MDAMB468-luc cells showed similar brightness (Figure 1C). These signals were completely blocked by the addition of excess cetuximab or panitumumab, suggesting that the conjugated mAbs specifically bind to the same epitope on EGFR, confirming previous results (Koefoed et al., 2011; Salfeld, 2007) (Supplementary Figure 1). Therefore, both cet-IR700 and pan-IR700 display similar fluorescence intensity, and bind to the same epitope of EGFR.

Serial imaging with fluorescence microscopy showed that the two antibody conjugates behaved similarly after binding to EGFR antigens on the cell surface. After 1 h incubation, both cet-IR700 and pan-IR700 localized on the cell membrane and early internalization was observed whereby IR700 fluorescence co-localized with the fluorescence of lysotracker in EGFR-positive A431 or MDAMB468-luc cells (Figure 1D). After 6 h incubation, both the fluorescence of cet-IR700 and pan-IR700 increasingly internalized into the lysosome, which co-localized with lysotracker. Thus, both agents behaved similarly after binding to EGFR.

3.2. *Identical* in vitro *photoimmunotherapy effects were observed with cet-IR700 and pan-IR700*

Serial fluorescence microscopy was performed after PIT with cet-IR700 and pan-IR700 to compare their *in vitro* efficacy. Immediately after exposure to NIR light (25 mW/cm^2 for 80 s resulting in a light dose of 2 J/cm^2) cellular swelling, bleb formation and rupture of the lysosome were observed in both A431 and MDAMB468-luc cells incubated with either cet-IR700 or pan-IR700 (Figure 2A and Supplementary Video 1–4). Most of these cellular changes were observed within 30 min of light exposure (Supplementary Video 1–4), indicating rapid induction of necrotic cell death after PIT. No significant differences in the initiation time for cellular changes or the severity of the cellular damage was observed between treatments with the two conjugates, suggesting that both agents induce profound cell necrosis after PIT.

Supplementary video related to this article can be found at http://dx.doi.org/10.1016/j.molonc.2014.01.006.

In order to examine the effects of *in vitro* PIT quantitatively, we performed a cytotoxicity assay with PI staining and a luciferase activity assay. Based on incorporation of PI, percentage of cell death increased in a light dose dependent manner. There was no significant cytotoxicity associated with NIR light alone in the absence of either agent. Mild cytotoxicity was observed when the cells were exposed to the conjugates alone without light (Figure 2B and C). No significant difference was detected between treatments with cet-IR700 and pan-IR700 with regard to quantitative measures of necrosis. The luciferase activity assay in MDAMB468-luc cells showed significant decreases of relative light units (RLU) related to PIT-induced reductions in ATP production in living cells, indicating a decrease in cellular activity which was dose dependent (Figure 2D). These studies suggest that both conjugates have identical efficacy in inducing rapid necrotic cell death after *in vitro* PIT.

The efficacy of *in vitro* PIT was also examined with A431 3D spheroids (Dubessy et al., 2000; Graff and Wittrup, 2003; Laderoute et al., 1992; Waleh et al., 1994). Compared to conventional monolayer cell cultures, 3D spheroids resemble real tissues better in terms of structural and functional properties. Since we use mAb-IR700 conjugates to target cancer

Figure 4 – Cet-IR700 and pan-IR700 demonstrate differences in *in vivo* effects of PIT. (A) Repeated cet-IR700 mediated PIT leads to less effective A431 tumor volume reduction than pan-IR700 (cet-IR700 PIT group vs. pan-IR700 PIT group after day 12: $p < 0.0001$) ($n = 10$ mice in each treatment group; $^*P < 0.0001$, by Kruskal–Wallis test with post-test). The treatment regimen is shown below the graph. (B) Repeated cet-IR700 mediated PIT leads to less prolonged survival in A431 tumor bearing mice than with pan-IR700 (cet-IR700 PIT group vs. pan-IR700 PIT group: $p < 0.01$) ($n = 10$ mice in each treatment group; $^{**}P < 0.0001$, by Long-rank test and Wilcoxon test). (C) Repeated PIT with pan-IR700 leads to less bioluminescence at 6 h, 3 day, and 4 day after the treatment than cet-IR700 ($n = 7$ mice in each treatment group; cet-IR700 PIT group vs. pan-IR700 PIT group: $^{***}P < 0.01$, $^{****}P < 0.05$). The treatment regimen and time points of measurement of bioluminescence are indicated on the left of the graph. (D) Bioluminescence images of MDAMB468-luc orthotopic tumors in response to repeated PIT with cet-IR700 or pan-IR700. Selected mice that had almost the same tumor relative light unit (RLU) before therapy are shown (cet-IR700; 5479 counts/tumor, pan-IR700; 5977 counts/tumor). (E) Fluorescence images obtained at each time point before and after repeated PIT. (F) I*n vivo* fluorescence imaging of a A431 xenograft and (G) MDAMB468-luc orthotopic breast tumor bearing mice treated with repeated PIT showed differences in fluorescence signals in the tumors between treatments with cet-IR700 and pan-IR700. Tumors of almost equal size were selected (see magnified view). (H) Tumor-to-background ratio (TBR) of the IR700 fluorescence intensity in A431 tumors or MDAMB468-luc orthotopic breast tumors showed a difference in quantitative uptake and retention (A431; $n = 10$ mice in each treatment group; $^*P < 0.05$) (MDAMB468-luc; $n = 7$ mice in each treatment group).

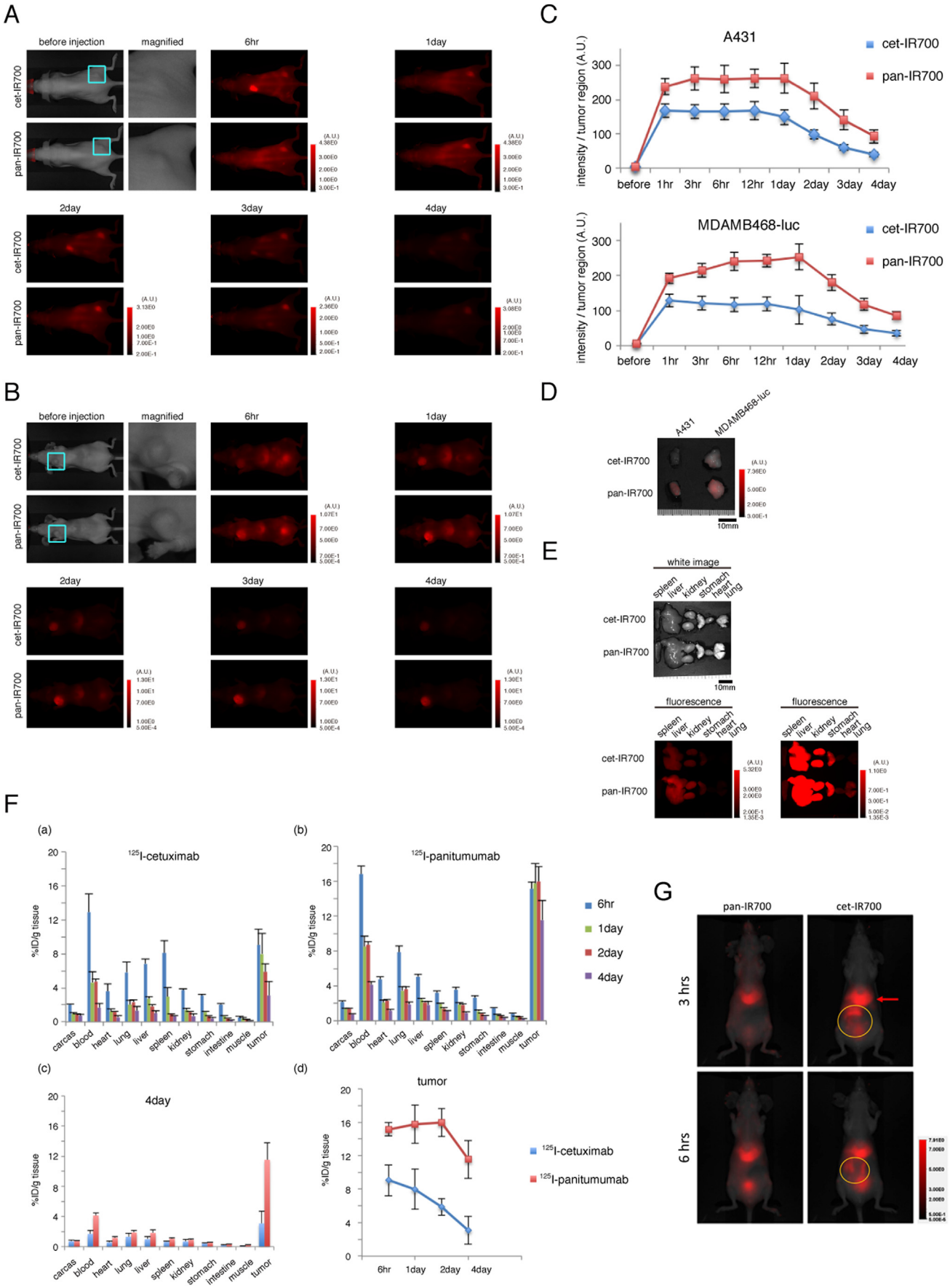
A
before injection
magnified
6hr
1day
2day
3day
4day
cet-IR700
pan-IR700
B
C
A431
MDAMB468-luc
cet-IR700
pan-IR700
intensity / tumor region (A.U.)
before 1hr 3hr 6hr 12hr 1day 2day 3day 4day
D
A431
MDAMB468-luc
10mm
E
white image
fluorescence
spleen liver kidney stomach heart lung
F
(a)
125I-cetuximab
(b)
125I-panitumumab
%ID/g tissue
carcas blood heart lung liver spleen kidney stomach intestine muscle tumor
6hr
1day
2day
4day
(c)
4day
(d)
tumor
6hr 1day 2day 4day
125I-cetuximab
125I-panitumumab
G
pan-IR700
cet-IR700
3 hrs
6 hrs

cells, the penetration of conjugates to the cancer tissue is critical for successful PIT. Permeation of cet-IR700 and pan-IR700 into the spheroids was examined by microscopy. The outer layer of the spheroids was stained by the conjugates after 1 h co-incubation and the stained area spread centripetally in a time dependent manner (Figure 3A). Quantification of IR700 fluorescence intensity of either agent within spheroids showed no significant difference (Figure 3B), suggesting that both agents permeated within 3D culture cells at the same rate.

To visualize and quantify the effects of PIT in the 3D spheroid model, concurrent microscopic observation and LDH cytotoxicity assay was performed (Lee et al., 2011). At 1 h post-PIT, there was a physical swelling of the spheroids (Figure 3C). The outer layer of the spheroid was stained with PI, indicating cell death where NIR light penetrated. The LDH cytotoxicity assay again showed significant cell death that was light dose dependent but an absence of cell death without agents or with light alone and mild cytotoxicity using either conjugate alone (Figure 3D), which conforms to the results in 2D cell cultures (Figure 2B and C). No significant difference between treatments with cet-IR700 or pan-IR700 was detected in serial microscopic observations (data not shown) or the LDH cytotoxicity assay in the 3D spheroid model (Figure 3D). These results revealed that cet-IR700 and pan-IR700 could induce similar effects of PIT *in vitro*, not only in 2D but also in 3D cell cultures, and show similar penetration within 3D spheroids.

3.3. *Pan-IR700 is superior to cet-IR700 for* in vivo *photoimmunotherapy*

We compared the two conjugates for their *in vivo* PIT effects using A431 xenografts and orthotopically grafted MDAMB468-luc tumors. Contrary to the *in vitro* PIT results, significant differences in the efficacy of cet-IR700 and pan-IR700 were observed in A431 xenograft mice undergoing PIT (Figure 4A and B). Tumor volume was reduced and survival was prolonged significantly in the pan-IR700 PIT group compared with the cet-IR700 PIT group (tumor volume; pan-IR700 PIT group vs. cet-IR700 PIT group after day 12: $p < 0.0001$ (Kruskal–Wallis test with post-test), overall survival; pan-IR700 PIT group vs. cet-IR700 PIT group: $p < 0.01$ (long-rank test and Wilcoxon test)). Mice injected with either cet-IR700 or pan-IR700 alone showed minimal tumor growth inhibition and no therapeutic effect in the survival study. We also examined the therapeutic effect of *in vivo* PIT by bioluminescence quantification (Figure 4C and D). The RLU ratio, (post-PIT RLU to pre-PIT RLU), in MDAMB468-luc orthotopic breast tumors demonstrated that the pan-IR700 group had significant decreases at 6 h after PIT (***$p < 0.01$), while the RLU ratio in the cet-IR700 group was unchanged (Figure 4C). Although the RLU ratio in the cet-IR700 PIT group also decreased within 2 days after PIT probably due to the accumulated damage to the tumors but returned to the baseline level at 3 days after PIT (ns, 1day; $P = 0.078$, 2day; $p = 0.183$). Thus, the pan-IR700 was more effective as an *in vivo* PIT agent than cet-IR700. Importantly, after only a single irradiation at 100 J/cm^2 to MDAMB468-luc tumors, both cet-IR700 and pan-IR700 had similar decreases in the RLU ratio (Supplementary Figure 2); differences between the two agents were more effectively demonstrated after repeated exposures to light indicating that pharmacokinetics of the two conjugates may be critical in determining their efficacy as PIT agents.

To further elucidate the difference in *in vivo* therapeutic effects of PIT between cet-IR700 and pan-IR700, serial fluorescence images of the tumor-bearing mice were assessed before and after each light exposure (day 1 and day 2) and 1 day after the last irradiation (Figure 4E). One day after injection of the agents, pan-IR700 showed higher fluorescence intensity than cet-IR700 in both A431 and MDAMB468-luc tumors (Figure 4F (a) and G (a)). IR700 fluorescence signal was compromised due to washing out from dead cells and partial photo-bleaching after exposure to 50 J/cm^2 of NIR light (Figure 4F (b, d) and G (b, d)). Pan-IR700 showed consistently higher intensity in tumors than cet-IR700 after each irradiation (Figure 4F (c, e) and G (c, e)), suggesting that pan-IR700 accumulated and was retained in tumors to a higher degree than cet-IR700 over the first 3 days after injection. TBR also indicated higher accumulation of pan-IR700 in tumors compared to cet-IR700 one day after NIR light exposure (Figure 4H). These results may help explain the differences in therapeutic effects between the two conjugates as they may relate to their respective pharmacokinetics.

3.4. *Differences in biodistribution between cet-IR700 and pan-IR700*

To examine the differences in pharmacokinetics, serial IR700 fluorescence imaging was performed after injection of cet-IR700 or pan-IR700 and a biodistribution study utilizing ^{125}I-labeled versions of each conjugate was performed in EGFR-positive tumor-bearing mice. Both A431 and MDAMB468-luc

Figure 5 – *In vivo* fluorescence imaging of tumor bearing mice and biodistribution. *In vivo* fluorescence imaging of A431 xenografts (A) or MDAMB468-luc orthotopic tumor bearing mice (B) treated with cet-IR700 or pan-IR700 (only intravenous injection, without NIR irradiation). To demonstrate the difference of fluorescence signals between treatments of the two agents, the signal window was set at each period. Quantitative analysis of IR700 fluorescence signals in A431/MDAMB468-luc tumors (C) showed significantly higher intensity with pan-IR700 than with cet-IR700 from 3 h to 3 day after injection ($n = 5$ mice in each group; $P < 0.05$). *Ex vivo* fluorescence images of A431 or MDAMB468-luc tumor (D) and organs (E) at 4 day after injection also showed higher intensity with pan-IR700 than with cet-IR700. (F) *In vivo* biodistribution of radioactivity at 6 h, 1 day, 2 day and 4 day after injection of ^{125}I-cetuximab (a) and ^{125}I-panitumumab (b) into A431 tumor bearing mice, and biodistribution at day 4 after injection was compared between these two agents (c). Radioactivity in the tumor (d) was significantly higher with ^{125}I-panitumumab than with ^{125}I-cetuximab from 6 h to 4 day after injection ($n = 5$ mice in each group; $P < 0.05$ at each sampling point). (G) *In vivo* IR700 fluorescence images show higher hepatic and splenic accumulation (red arrow) followed by biliary excretion (yellow circle) of cet-IR700 than that of pan-IR700 at 3 and 6 h.

tumors showed higher fluorescence intensity with pan-IR700 than cet-IR700 at all time points. Furthermore, pan-IR700 showed higher fluorescence intensity in the background than cet-IR700 in both animal models (Figure 5A and B). Quantification of fluorescence in both tumors also showed higher intensity in the pan-IR700 group than in the cet-IR700 group, and a trend toward an earlier decrease of signals in the cet-IR700 than in the pan-IR700 group (Figure 5C). High fluorescence signals in the intestine were observed only in mice injected with cet-IR700 6 h after injection (Figure 5B), suggesting earlier hepatic catabolism and biliary excretion of cet-IR700 than pan-IR700. In non-tumor bearing mice, fluorescence signals in the intestine were observed as early as 1 h after injection (Supplementary Figure 3). With *ex vivo* imaging at 4 day after injection, higher fluorescence signals were observed within tumors and organs in mice injected with pan-IR700 than with cet-IR700 (Figure 5D and E).

Biodistribution studies showed higher accumulation of radioactivity in A431 tumors in the ^{125}I-panitumumab group than the ^{125}I-cetuximab group at all time points (Figure 5F (a–d)). Higher radioactivity was shown in the liver, spleen, and intestine at 6 h after injection in the ^{125}I-cetuximab group, suggesting earlier catabolism of cetuximab in the liver. Higher hepatic and splenic accumulation followed by biliary excretion was found with cet-IR700 compared to pan-IR700 at 3 and 6 h using IR700 fluorescence images (Figure 5G). At 4 day after injection, radioactivity in the organs, tumors and blood was higher in the ^{125}I-panitumumab group than in the ^{125}I-cetuximab group (Figure 5F (c)), consistent with the *ex vivo* fluorescence images (Figure 5D and E). These results suggest that panitumumab has slower clearance and higher accumulation in tumor bearing mice than cetuximab over a period of 4 days, which may explain the superior effects of pan-IR700 with *in vivo* PIT. On the other hand, cetuximab was more rapidly catabolized in the liver, resulting in less accumulation of cet-IR700 in tumors, thus compromising the PIT effects *in vivo*.

4. Discussion

The term, “PIT”, was first used in studies employing antibody-photosensitizer conjugates three decades ago (Mew et al., 1983). Although we have adopted the same name, the design of the immunoconjugate is different in a key respect. In the original “PIT”, antibodies were conjugated to very hydrophobic photosensitizers used for photodynamic therapy (PDT). The pharmacokinetic properties of the conjugate were dominated by the hydrophobicity of the photosensitizer, thus, limiting delivery to the tumor compared to background, resulting in poorly targeted uptake, leading to minor gains in efficacy compared with “untargeted” hydrophobic photosensitizers. The PIT we describe, while similar in concept to the original PIT, has completely different pharmacokinetic properties since the photosensitizer is highly hydrophilic and therefore, requires the antibody for targeting. This enables highly targeted accumulation at the tumor with minimal uptake in non-target tissue. Therefore, the current PIT described in this study is a new class of therapy based on targeted hydrophilic photosensitizers.

Cetuximab and panitumumab are both widely used mAbs in tumors expressing EGFR and both are considered suitable candidates as PIT conjugates. We show that cet-IR700 and pan-IR700 bind to EGFR-expressing cancer cells in *in vitro* culture with nearly identical affinity and both agents are capable of penetrating into 3D spheroids. Predictably, these properties result in nearly identical *in vitro* PIT-induced cytotoxicity. In contrast, pan-IR700 was superior to cet-IR700 as an *in vivo* PIT agent owing to its more favorable pharmacokinetics in mouse models. Optimizing the fractionation schedule did not alter these results, although to some extent the deficiencies of cet-IR700 can be overcome by increasing the light dose.

An important aspect of PIT is that after the first exposure to NIR light, there are rapid and dramatic increases in vascular permeability to nano-sized molecules such as antibodies. PIT only targets tumor cells and thus leaves the vessels intact and thus, blood flow is at least maintained. Moreover, the first cells to be killed by PIT are perivascular tumor cells, thus creating a potential space just outside blood vessels that is permissive to leakage into the extravascular space (Sano et al., 2013c). After the first PIT session, circulating antibody-IR700 conjugates can permeate deeply into the treated tumor’s extravascular space where they become even more effective as PIT agents after the second exposure to light. Previous measurements have suggested that this super enhanced permeability and retention (SUPR) effect can result in a 20-fold increase in the delivery of nano-sized molecules compared to baseline. This promotes homogeneous redistribution of antibody-IR700 conjugates within the tumor after the initial PIT treatment (Sano et al., 2013c). The prolonged retention of the pan-IR700 conjugate in the circulation, therefore, increases the efficacy of pan-IR700 relative to cet-IR700 which has a shorter circulatory half life. Radiolabeled cetuximab showed faster clearance from the circulation and higher hepatic accumulation than panitumumab. Cet-IR700 and radiolabeled cetuximab showed similarly high hepatic accumulations. This difference might derive from the difference in species or protein class characteristics of cetuximab and panitumumab, which are respectively, chimeric (13% mouse and 87% human) IgG1 and human (100% human) IgG2 monoclonal antibodies (Salfeld, 2007). To the extent that the pharmacokinetics in humans might differ from that shown in mice, this pharmacokinetic disadvantage of cet-IR700 may be less of a problem in humans. However, this study clearly suggests that longer retention in the circulation is an advantageous feature of a PIT agent as it permits more tumor accumulation, especially after the first PIT session. These findings should inform the decision regarding which conjugate to use when considering early phase human trials of PIT.

5. Conclusions

Although cet-IR700 and pan-IR700 showed identical binding and therapeutic PIT effects *in vitro*, pan-IR700 showed superior therapeutic tumor effects in *in vivo* mice models compared to cet-IR700 due to differences in the pharmacokinetics of the

two antibodies. These findings could inform the selection of suitable antibody-IR700 conjugates for human clinical trials.

Author contributions

K.S. mainly conducted experiments, performed analysis and wrote the manuscript; R.W., H.H., T.H., T.N., I.K. and C.H.P. conducted experiments and performed analysis; P.L.C. wrote the manuscript and supervised the project; and H.K. planned and initiated the project, designed and conducted experiments, wrote the manuscript, and supervised the entire project.

Conflict of interest

PC and HK hold a patent on photoimmunotherapy.

Acknowledgments

This research was supported by the Intramural Research Program of the National Institutes of Health, National Cancer Institute, Center for Cancer Research. K.S. is supported with JSPS Research Fellowship for Japanese Biomedical and Behavioral Researchers at NIH.

Appendix A. Supplementary data

Supplementary data related to this article can be found at http://dx.doi.org/10.1016/j.molonc.2014.01.006.

REFERENCES

Dubessy, C., Merlin, J.M., Marchal, C., Guillemin, F., 2000. Spheroids in radiobiology and photodynamic therapy. Crit. Rev. Oncol. Hematol. 36, 179–192.

Eng, C., 2010. The evolving role of monoclonal antibodies in colorectal cancer: early presumptions and impact on clinical trial development. Oncologist 15, 73–84.

Gialeli, C., Kletsas, D., 2009. Targeting epidermal growth factor receptor in solid tumors: critical evaluation of the biological importance of therapeutic monoclonal antibodies. Curr. Med. Chem. 29, 3797–3804.

Graff, C.P., Wittrup, K.D., 2003. Theoretical analysis of antibody targeting of tumor spheroids: importance of dosage for penetration, and affinity for retention. Cancer Res. 63, 1288–1296.

Koefoed, K., Steinaa, L., Søderberg, J.N., Kjær, I., Jacobsen, H.J., Meijer, P.-J., Haurum, J.S., Jensen, A., Kragh, M., Andersen, P.S., Pedersen, M.W., 2011. Rational identification of an optimal antibody mixture for targeting the epidermal growth factor receptor. MAbs 3, 584–595.

Laderoute, K.R., Murphy, B.J., Short, S.M., Grant, T.D., Knapp, A.M., Sutherland, R.M., Park, M., 1992. Enhancement of transforming growth factor-a. Synthesis in multicellular tumour spheroids of A431 squamous carcinoma cells. Br. J. Cancer 2, 157–162.

Lee, S.Y., Jeon, H.M., Kim, C.H., Ju, M.K., Bae, H.S., Park, H.G., Lim, S.-C., Han, S.I., Kang, H.S., 2011. Homeobox gene Dlx-2 is implicated in metabolic stress-induced necrosis. Mol. Cancer 10, 113.

Markovic, A., Chung, C.H., 2012. Current role of EGF receptor monoclonal antibodies and tyrosine kinase inhibitors in the management of head and neck squamous cell carcinoma. Expert Rev. Anticancer Ther. 12, 1149–1159.

Mew, D., Wat, C., Towers, G.H.N., Levy, J.G., 1983. Photoimmunotherapy: treatment of animal tumors with tumor-specific. J. Immunol. 130, 1473–1477.

Mitsunaga, M., Nakajima, T., Sano, K., Choyke, P.L., Kobayashi, H., 2012a. Near-infrared theranostic photoimmunotherapy (PIT): repeated exposure of light enhances the effect of immunoconjugate. Bioconjug. Chem. 23, 604–609.

Mitsunaga, M., Nakajima, T., Sano, K., Kramer-Marek, G., Choyke, P.L., 2012b. Immediate in vivo target-specific cancer cell death after near infrared photoimmunotherapy. BMC Cancer 12, 1.

Mitsunaga, M., Ogawa, M., Kosaka, N., Rosenblum, L.T., Choyke, P.L., 2011. Cancer cell – selective in vivo near infrared photoimmunotherapy targeting specific membrane molecules. Nat. Med. 17, 1685–1691.

Nakajima, T., Sano, K., Choyke, P.L., Kobayashi, H., 2013. Improving the efficacy of photoimmunotherapy (PIT) using a cocktail of antibody conjugates in a multiple antigen tumor model. Theranostics 3, 357–365.

Nakajima, T., Sano, K., Mitsunaga, M., Choyke, P.L., Kobayashi, H., 2012. Real-time monitoring of in vivo acute necrotic cancer cell death induced by near infrared photoimmunotherapy using fluorescence lifetime imaging. Cancer Res. 72, 4622–4628.

Norguet, E., Dahan, L., Seitz, J.-F., 2012. Targeting esophageal and gastric cancers with monoclonal antibodies. Curr. Top. Med. Chem. 12, 1678–1682.

Ogawa, M., Regino, C.A.S., Seidel, J., Green, M.V., Xi, W., Williams, M., Kosaka, N., Choyke, P.L., Kobayashi, H., 2009. Dual-modality molecular imaging using antibodies labeled with activatable fluorescence and a radionuclide for specific and quantitative targeted cancer detection. Bioconjug. Chem. 20, 2177–2184.

Raben, N., Shea, L., Hill, V., Plotz, P., 2009. Monitoring Autophagy in Lysosomal Storage Disorders, first ed.. In: Methods in Enzymology Elsevier Inc.

Reichert, J.M., Rosensweig, C.J., Faden, L.B., Dewitz, M.C., 2005. Monoclonal antibody successes in the clinic. Nat. Biotechnol. 23, 1073–1078.

Salfeld, J.G., 2007. Isotype selection in antibody engineering. Nat. Biotechnol. 25, 1369–1372.

Sano, K., Mitsunaga, M., Nakajima, T., Choyke, P.L., Kobayashi, H., 2013a. Acute cytotoxic effects of photoimmunotherapy assessed by 18F-FDG PET. J. Nucl. Med. 54, 770–775.

Sano, K., Nakajima, T., Ali, T., Bartlett, D.W., Wu, A.M., Kim, I., Paik, C.H., Choyke, P.L., Kobayashi, H., 2013b. Activatable fluorescent cys-diabody conjugated with indocyanine green derivative: consideration of fluorescent catabolite kinetics on molecular imaging. J. Biomed. Opt. 18, 101304.

Sano, K., Nakajima, T., Choyke, P.L., Kobayashi, H., 2013c. Markedly enhanced permeability and retention effects induced by photoimmunotherapy of tumors. ACS Nano 7, 717–724.

Sano, K., Nakajima, T., Miyazaki, K., Ohuchi, Y., Ikegami, T., Choyke, P.L., Kobayashi, H., 2013d. Short PEG-linkers improve the performance of targeted, activatable monoclonal antibody-indocyanine green optical imaging probes. Bioconjug. Chem. 24, 811–816.

Sato, K., Watanabe, T., Wang, S., Kakeno, M., Matsuzawa, K., Matsui, T., Yokoi, K., Murase, K., Sugiyama, I., Ozawa, M., Kaibuchi, K., 2011. Numb controls E-cadherin endocytosis

through p120 catenin with aPKC. Mol. Biol. Cell 22, 3103–3119.
Smith, S.M., Flentke, G.R., Garic, A., 2012. Developmental toxicology. Methods Mol. Biol. 889, 85–103.
Stinchcombe, T.E., Socinski, M.A., 2010. Targeted therapies: biomarkers in NSCLC for selecting cetuximab therapy. Nat. Rev. Clin. Oncol. 7, 426–428.
Tebbutt, N., Pedersen, M.W., Johns, T.G., 2013. Targeting the ERBB family in cancer: couples therapy. Nat. Rev. Cancer 13, 663–673.
Tung, Y.-C., Hsiao, A.Y., Allen, S.G., Torisawa, Y., Ho, M., Takayama, S., 2011. High-throughput 3D spheroid culture and drug testing using a 384 hanging drop array. Analyst 136, 473–478.
Vecchione, L., Jacobs, B., Normanno, N., Ciardiello, F., Tejpar, S., 2011. EGFR-targeted therapy. Exp. Cell Res. 317, 2765–2771.
Waldmann, T.A., 2003. Immunotherapy: past, present and future. Nat. Med. 9, 269–277.
Waleh, N.S., Gallo, J., Grant, T.D., Murphy, B.J., Kramer, R.H., Sutherland, R.M., 1994. Selective down-regulation of integrin receptors in spheroids of squamous cell carcinoma. Cancer Res. 54, 838–843.
Yamaguchi, H., Chang, S.-S., Hsu, J.L., Hung, M.-C., 2013. Signaling cross-talk in the resistance to HER family receptor targeted therapy. Oncogene, 1–9.
Yarden, Y., Pines, G., 2012. The ERBB network: at last, cancer therapy meets systems biology. Nat. Rev. Cancer 12, 553–563.